J|A|C|S
ARTICLES
Published on Web 08/20/2002

A Novel Approach for the Sequential Backbone Assignment of Larger Proteins: Selective Intra-HNCA and DQ-HNCA

Daniel Nietlispach,*,† Yutaka Ito,‡ and Ernest D. Laue†

Contribution from the Cambridge Centre for Molecular Recognition, Department of Biochemistry, University of Cambridge, 80 Tennis Court Road, Cambridge CB2 1GA, U.K., and Cellular and Molecular Biology Laboratory, RIKEN, 2-1 Hirosawa, Wako, Saitama 351-0198, Japan

Received February 8, 2002

Abstract: Sequential assignment of backbone resonances in larger proteins can be achieved by recording two or more complementary triple-resonance NMR spectra of deuterated proteins. For such proteins, higher fields and experiments based on the TROSY method provide the needed resolution and sensitivity. However, increasingly rapid carbonyl relaxation at the high magnetic field strengths required by TROSY techniques renders assignment strategies that rely on sequential HN(CO)CA-type experiments much less efficient for proteins >40 kDa. Here we present two complementary new experiments, which allow backbone assignments with good sensitivity for larger deuterated proteins. A 3D intra-HNCA experiment provides uniquely the intraresidue connection, while a 3D DQ-HNCA experiment, which detects a $^{13}C^{\alpha}_{i}{}^{13}C^{\alpha}_{i-1}$ double-quantum (DQ) coherence, contains the sequential information. The experiments work well at high magnetic fields, and their utility is demonstrated on a protein with a correlation time of 28 ns (~60 kDa). For larger proteins the sensitivity is predicted through simulations which suggest that the approach should work for proteins with correlation times >50 ns.

Introduction

The sequential assignment of the protein backbone resonances is usually one of the first tasks to be carried out during protein structure determination by NMR and is reliant on recording experiments that correlate the chemical shifts of ^{1}HN, ^{15}N, $^{13}C^{\alpha}$, $^{13}C^{\beta}$, and $^{13}C'$ nuclei.[1,2] Typically, two neighboring residues are identified through analysis of pairwise complementary 3D NMR experiments which allow one to establish a connection through the match of the $^{13}C^{\alpha}$ chemical shifts of residues i and $i-1$ to the shifts of the ^{1}HN and ^{15}N spins of the ith residue.[3,4] Over the years a large number of experiments have been developed to accomplish this, but as the sensitivity of triple-resonance experiments decreases rapidly with increasing molecular size, the number which give practical sensitivity with larger proteins is greatly reduced. Major challenges to NMR studies of larger proteins also come from the higher degree of crowding due to the increasing number of resonances in the spectra. The introduction of deuteration in combination with efficient ^{13}C and ^{15}N labeling techniques[5,6] has improved both resolution and sensitivity and allowed a substantial increase in the size of proteins which can be investigated. In many cases the complementary 3D HNCA/HN(CO)CA[3,7−9] experiments are the most appropriate choice for this sequential assignment procedure. Assignments of proteins with up to 370 amino acids have been reported in the literature.[10,11] The more recent introduction by Pervushin and co-workers of relaxation-compensated TROSY techniques,[12,13] in combination with deuteration, has allowed this size limit to be pushed even further. With the help of TROSY-enhanced triple-resonance experiments[14−17] the sequential backbone assignments of proteins as large as 100 kDa

* To whom correspondence should be addressed. Fax: (+44) 01223 766002. E-mail: dn0@bioc.cam.ac.uk.
† University of Cambridge.
‡ On leave from RIKEN.

(1) Bax, A. *Curr. Opin. Struct. Biol.* **1994**, *4*, 738−744.
(2) Cavanagh, J.; Fairbrother, W. J.; Palmer, A. G.; Skelton, N. J. *Protein NMR Spectroscopy: Principles and Practice*; Academic Press: San Diego, 1996.
(3) Ikura, M.; Kay, L. E.; Bax, A. *Biochemistry* **1990**, *29*, 4659−4667.
(4) Kay, L. E.; Ikura, M.; Tschudin, R.; Bax, A. *J. Magn. Reson.* **1990**, *89*, 496−514.
(5) LeMaster, D. *Prog. NMR Spectrosc.* **1994**, *26*, 371−419.
(6) Gardner, K. H.; Kay, L. E. *Annu. Rev. Biophys. Biomol. Struct.* **1998**, *27*, 357−406.
(7) Grzesiek, S.; Bax, A. *J. Magn. Reson.* **1992**, *96*, 432−440.
(8) Yamazaki, T.; Lee, W.; Revington, M.; Mattiello, D. L.; Dahlquist, F. W.; Arrowsmith, C. H.; Kay, L. E. *J. Am. Chem. Soc.* **1994**, *116*, 6464−6465.
(9) Yamazaki, T.; Lee, W.; Arrowsmith, C. H.; Muhandiram, D. R.; Kay, L. E. *J. Am. Chem. Soc.* **1994**, *116*, 11655−11666.
(10) Shan, X.; Gardner, K. H.; Muhandiram, D. R.; Kay, L. E.; Arrowsmith, C. H. *J. Biomol. NMR* **1998**, *11*, 307−318.
(11) Gardner, K. H.; Zhang, X. C.; Gehring, K.; Kay, L. E. *J. Am. Chem. Soc.* **1998**, *120*, 11738−11748.
(12) Pervushin, K.; Riek, R.; Wider, G.; Wuthrich, K. *Proc. Natl. Acad. Sci. U.S.A.* **1997**, *94*, 12366−12371.
(13) Pervushin, K. *Q. Rev. Biophys.* **2000**, *33*, 161−197.
(14) Salzmann, M.; Pervushin, K.; Wider, G.; Senn, H.; Wuthrich, K. *Proc. Natl. Acad. Sci. U.S.A.* **1998**, *95*, 13585−13590.
(15) Salzmann, M.; Wider, G.; Pervushin, K.; Senn, H.; Wuthrich, K. *J. Am. Chem. Soc.* **1999**, *121*, 844−848.
(16) Yang, D. W.; Kay, L. E. *J. Biomol. NMR* **1999**, *13*, 3−10.
(17) Loria, J. P.; Rance, M.; Palmer, A. G. *J. Magn. Reson.* **1999**, *141*, 180−184.

have been published.[18] While for intermediate-sized proteins resonance overlap in the ^{13}C dimension can be reduced by the introduction of a constant time[19−21] period, a 4D resolved HNCACO/HNCOCA[22]-based approach was shown to be more suitable for proteins with correlation times >40 ns.

Transverse-relaxation-compensated techniques involving the ^{1}HN and ^{15}N nuclei benefit most from the highest magnetic field strength available,[12] but unfortunately the carbonyl transverse-relaxation rate also increases in a manner that is approximately proportional to the square of the static magnetic field strength employed. This leads to a situation where the sensitivity of crucial experiments such as the HN(CO)CA deteriorates and the technique begins to perform better at lower fields,[17] a situation where the achievable spectral resolution and overall sensitivity may be insufficient. The time periods in experiments during which carbonyl spins are transverse must therefore be kept to a minimum. In this context, Permi et al. proposed an elegant HNCA experiment[23] which allows the discrimination of intra- and interresidue connections on the basis of unequal i and $i - 1$ cross-peak multiplicities in the $^{13}C^{\alpha}$ dimension. Meissner and co-workers chose a different approach, showing that interresidue connections can be obtained from a modified sequential HNCA experiment.[24]

We describe in this paper a pair of sensitive new TROSY-based HNCA-type experiments which provide a new approach for backbone assignment. The first, an intra-HNCA experiment, connects the ^{1}HN and ^{15}N resonances of residue i with the $^{13}C^{\alpha}$ resonance of the same residue only. The second, a double-quantum (DQ) HNCA experiment, correlates the ^{1}HN and ^{15}N of residue i with the sum of the frequencies of the $^{13}C^{\alpha}$ resonances of residues i and $i - 1$. For each amide proton, the interresidue $^{13}C^{\alpha}_{i-1}$ connection can then be obtained by subtraction of the corresponding $^{13}C^{\alpha}_{i}$ shift from the double-quantum frequency. This procedure can easily be integrated into a variety of assignment programs. The two complementary experiments allow the elucidation of the sequential assignment of the backbone of larger proteins, and form an alternative strategy to cases where the existing HNCA/HN(CO)CA[8,9]-based approach fails because of the low $i - 1$ signal intensity in the HN(CO)-CA. Alternatively, they can be used to complement existing HNCA spectra in cases where overlap or low sensitivity hinders sequential assignment. Spectral crowding in both new experiments is reduced by halving the number of cross-peaks compared to a conventional HNCA spectrum. In addition, the intra-HNCA experiment can also be implemented as a $^{1}HN/^{15}N/^{13}C^{\alpha}/^{13}C'$ 4D experiment without increasing the length of the pulse sequence. The sensitivity of these experiments and the practicality of this approach were tested at 800 MHz on a protein with a correlation time of 28 ns and shown to be superior to approaches which rely on the HN(CO)CA experiment or on a sequential-HNCA[24]-type experiment.

Materials and Methods

NMR Experiments. All spectra were recorded at 4 °C on a 1.0 mM sample of ^{15}N, ^{13}C, ^{2}H [Ile(δ_1 only), Leu, Val]-methyl-protonated[25,26] H-Ras (1−171)-GDP[27] in 20 mM phosphate buffer (pH 6.5), 40 mM sodium chloride, 5 mM magnesium chloride, 5 mM DTT, 0.01% NaN_3, and 10% D_2O added for lock stability regulation. Experiments were performed on Bruker DRX800 and DRX600 spectrometers equipped with four channels for the generation of ^{1}H, ^{13}C, ^{15}N, and ^{2}H pulses, a lock hold unit, and an actively shielded z-gradient coil. The 3D intra-HNCA and DQ-HNCA spectra were each recorded with 16 scans per increment and a relaxation delay of 1.6 s, resulting in a total experiment time of 29 h. Totals of 32, 24, and 512 complex data points were acquired in t_1, t_2, and t_3, respectively, corresponding to acquisition times of 5.5, 14.9, and 64 ms. For comparative purposes additional 3D HNCA,[8] HN(CO)CA,[9] and sequential-HNCA[24] experiments were recorded following published methods, using identical parameters and conditions. Data sets were processed using the AZARA[28] package and were analyzed in ANSIG[29] and AZARA. The ^{15}N dimension was extended by 40% using mirror image linear prediction.[30] Before Fourier transformation the data matrices were multiplied with a squared cosine-bell window function in ^{15}N and ^{13}C and a 60°-shifted sine-bell in the acquisition dimension. After linear prediction, zero-filling, and data reduction, the final matrix consisted of (128, 128, 1024) points. On the basis of TROSY-enhanced 2D ^{15}N T_1 and T_2 measurements, the correlation time of the H-Ras sample at 4 °C was determined to be 28 ± 0.5 ns.

Simulations. Magnetization transfer functions of the triple-resonance experiments shown in Figure 3 were computed, taking into account attenuation through relaxation, representative of a well-structured region of a isotropically tumbling protein, assuming an order parameter $S^2 = 0.85$ and an internal correlation time of 10 ps. For all simulated 3D experiments and for each correlation time and magnetic field strength represented, the individual transfer periods in the pulse sequences were adjusted to give the best transfer efficiencies. In Figures 2a and 3 the average magnitudes of the coupling constants were taken to be $^{1}J_{NC^a} = 11$ Hz, $^{2}J_{NC^a} = 7$ Hz, $^{1}J_{NC'} = 15$ Hz, $^{1}J_{C^aC'} = 55$ Hz, and $^{1}J_{C^aC^b} = 33$ Hz. Although the side chains of the protein are assumed to be highly deuterated, a residual dummy proton was introduced at a distance of 2.43 Å to the amide proton to mimic residual dipole−dipole contributions from surrounding protons in a typical α-helical environment. Relaxation of ^{15}N and $^{13}C^{\alpha}$ nuclei was treated using the isolated spin pair approximation and by considering dipolar and chemical shift anisotropy (CSA) autorelaxation terms.[2] Only contributions from the slowly relaxing $N_{tr}H^{\beta}$ and $H_{tr}N^{\beta}$ components were considered during the ^{15}N transfer periods and the ST2-PT[31] (single-transition to single-transition polarization transfer) coherence transfer steps. Carbonyl transverse relaxation was approximated by $R_2(C') = \tau_c(3/4 + B^2/150)$ as previously suggested by Bax et al.[32] The CSA values were assumed to be −165 ppm for ^{15}N and −9 ppm for ^{1}HN, with their principal axis tensor aligned collinear to the N−H bond vector.[33]

Theory

Figure 1a shows the pulse sequence of the new TROSY 3D intra-HNCA, which correlates the $^{1}HN_i$, $^{15}N_i$, and $^{13}C^{\alpha}_i$ nuclei,

(18) Salzmann, M.; Pervushin, K.; Wider, G.; Senn, H.; Wuthrich, K. *J. Am. Chem. Soc.* **2000**, *122*, 7543−7548.
(19) Vuister, G. W.; Bax, A. *J. Magn. Reson.* **1992**, *98*, 428−435.
(20) Santoro, J.; King, G. C. *J. Magn. Reson.* **1992**, *97*, 202−207.
(21) Shan, X.; Gardner, K. H.; Muhandiram, D. R.; Rao, N. S.; Arrowsmith, C. H.; Kay, L. E. *J. Am. Chem. Soc.* **1996**, *118*, 6570−6579.
(22) Yang, D. W.; Kay, L. E. *J. Am. Chem. Soc.* **1999**, *121*, 2571−2575.
(23) Permi, P.; Annila, A. *J. Biomol. NMR* **2001**, *20*, 127−133.
(24) Meissner, A.; Sorensen, O. W. *J. Magn. Reson.* **2001**, *150*, 100−104.
(25) Gardner, K. H.; Kay, L. E. *J. Am. Chem. Soc.* **1997**, *119*, 7599−7600.
(26) Rosen, M. K.; Gardner, K. H.; Willis, R. C.; Parris, W. E.; Pawson, T.; Kay, L. E. *J. Mol. Biol.* **1996**, *263*, 627−636.
(27) Kraulis, P. J.; Domaille, P. J.; Campbell-Burk, S. L.; Vanaken, T.; Laue, E. D. *Biochemistry* **1994**, *33*, 3515−3531.
(28) Boucher, W. Unpublished data.
(29) Kraulis, P. J. *J. Magn. Reson.* **1989**, *84*, 627−633.
(30) Zhu, G.; Bax, A. *J. Magn. Reson.* **1990**, *90*, 405−410.
(31) Pervushin, K.; Wider, G.; Wuthrich, K. *J. Biomol. NMR* **1998**, *12*, 345−348.
(32) Hu, J. S.; Bax, A. *J. Am. Chem. Soc.* **1997**, *119*, 6360−6368.
(33) Peng, J. W.; Wagner, G. In *Methods in Enzymology*; James, T. L., Oppenheimer, N., Eds.; Academic Press: San Diego, 1994; Vol. 239C, pp 563−596.

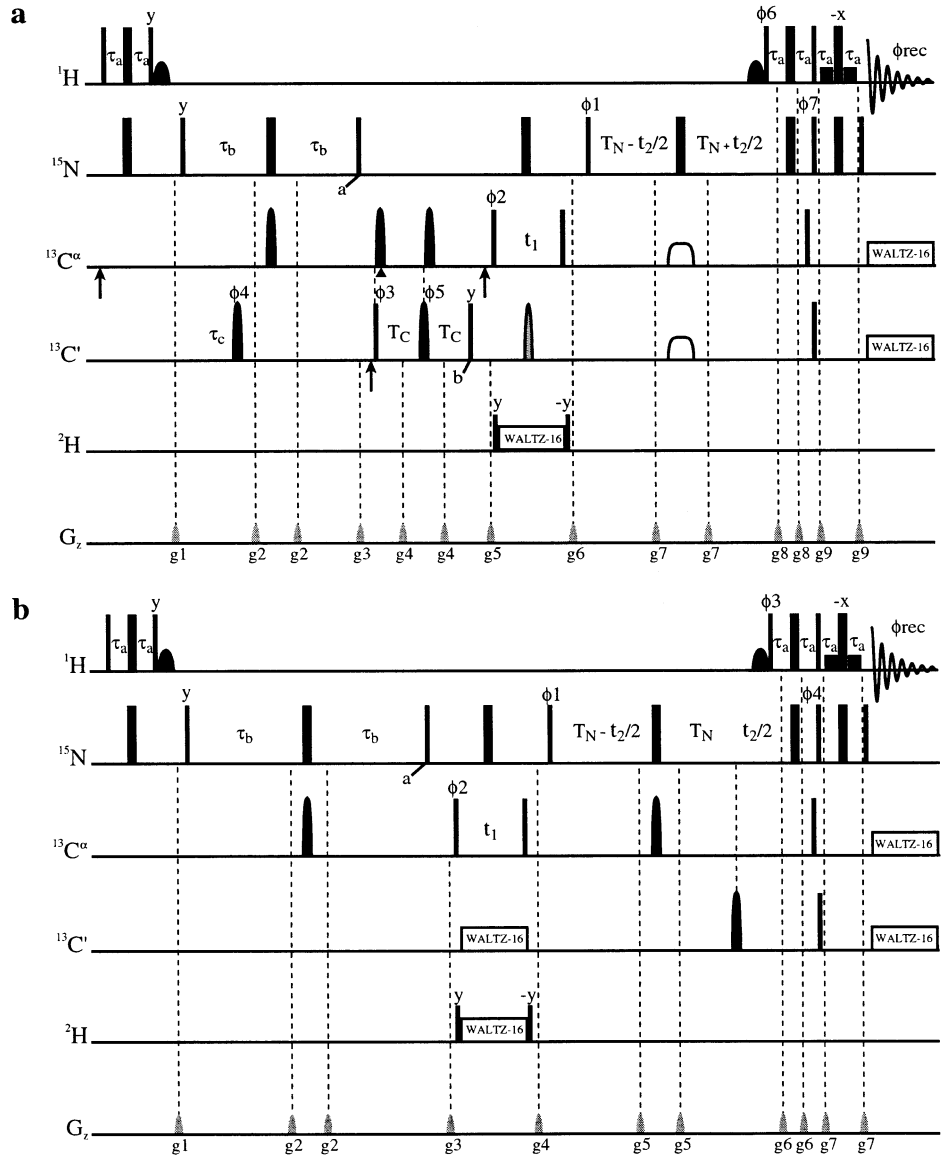

Figure 1. Experimental schemes for the intra-HNCA (a) and DQ-HNCA (b) experiments. Rectangular 90° and 180° pulses are indicated by thin and thick black vertical lines, respectively, where the phases are indicated above the pulses. Where no radio frequency phase is marked, the pulse is applied along *x*. Pulse phases are indicated for Bruker spectrometers to constructively add ^{1}HN and ^{15}N contributions to the ST2-PT coherence pathway.[31] The ^{1}H, ^{2}H, and ^{15}N carriers are set to 4.73 (water), 4.5, and 119.4 ppm, respectively. All proton pulses are applied with a field strength of 22 kHz with the exception of the shaped 90° pulse, which has the E-SNOB[41] profile (2.1 ms, 0.27 kHz) and the 1.4 ms 90° square low-power pulses of the WATERGATE[42] scheme. ^{15}N pulses employ a 6.3 kHz field, and ^{2}H 90° square pulses and the WALTZ-16[43] decoupling sequence are applied with a 0.8 kHz field. For the present case at 800 MHz, all rectangular 90° ^{13}C$^\alpha$ and ^{13}C′ pulses have a length of 40.1 μs to provide an excitation minimum at the corresponding ^{13}C′ and ^{13}C$^\alpha$ frequencies, respectively.[4] Decoupling of ^{13}C$^\alpha$ and ^{13}C′ spins during the acquisition time is achieved using a 60 ppm cosine-modulated WALTZ-16[43] field, centered at 116 ppm, employing pulses that have the SEDUCE-1[44] profile (300 μs 90° pulses, 3.6 kHz peak power). (a) The ^{13}C carrier is set to 56 ppm and moved to 176 ppm before the pulse with phase ϕ3 and switched back to 56 ppm immediately before the ^{13}C$^\alpha$ pulse with phase ϕ2. Arrows indicate the positions where the carrier is jumped. The black shaped 180° ^{13}C$^\alpha$ and ^{13}C′ pulses are applied with a G3[45] profile at a peak field strength of 9.0 kHz and have a duration of 400 μs. The position of the Bloch−Siegert compensation pulse is indicated by an arrowhead. The phase ϕ5 of the G3[45] pulse in the center of $2T_c$ is carefully adjusted to compensate for the phase changes which accompany the different power levels. The gray shaded ^{13}C′ 180° pulse is applied with a (sin *x*)/*x* shape profile (100 μs, 8.5 kHz). The two open shapes in the middle of $2T_N$ indicate a 180° pulse, applied as a single 375 μs adiabatic Chirp[46] sweep (60 kHz sweep width, 12.3 kHz peak power), centered at 100 ppm. The delays used are $\tau_a = 2.7$ ms, $\tau_b = 26$ ms, $\tau_c = 16.5$ ms, $T_C = 4.2$ ms, and $T_N = 15.8$ ms. The phase cycling is as follows: $\phi1 = (y, -y, -x, x)$, $\phi2 = 4(x), 4(-x)$, $\phi3 = 8(x), 8(-x)$, $\phi4 = 8(x), 8(-x)$, $\phi5 = x$, $\phi6 = y$, $\phi7 = y$, ϕrec $= (x, -x, y, -y), 2(-x, x, -y, y), (x, -x, y, -y)$. Frequency discrimination in the t_1(^{13}C$^\alpha$) dimension is achieved using States-TPPI[47] of ϕ3 and ϕ4, while in the t_2(^{15}N) dimension a phase-sensitive spectrum is obtained by recording a second FID for each increment of t_2, with $\phi1 = (y, -y, x, -x)$, and the phases of ϕ6 and ϕ7 inverted. For each successive t_2 value, ϕ1 and the phase of the receiver are incremented by 180°, and the data are processed as described by Kay et al.[48] The durations and strengths of the sine-shaped gradients are g1 = (1.1 ms, 11 G/cm), g2 = (0.7 ms, 4 G/cm), g3 = (1.0 ms, 5.5 G/cm), g4 = (0.6 ms, 4 G/cm), g5 = (1.3 ms, 12 G/cm), g6 = (1.5 ms, −17 G/cm), g7 = (0.5 ms, 11 G/cm), g8 = (0.9 ms, 17 G/cm), and g9 = (1.0 ms, 19 G/cm). (b) Many features are similar to the sequence above, and only differences are discussed. The carbon carrier is set to 48.5 ppm. The solid shaped 180° pulses are applied with a 400 μs G3[45] profile. Carbonyl decoupling during t_1 is achieved with WALTZ-16 using a 128 ppm cosine-modulated SEDUCE-1[44] profile (300 μs 90° pulse, centered at 56 ppm, 3.6 kHz peak power). The delays are $\tau_a = 2.7$ ms, $\tau_b = 25.5$ ms, and $T_N = 25.5$ ms. The phase cycling used is $\phi1 = (x, -x, y, -y)$, $\phi2 = 4(x), 4(y), 4(-x), 4(-y)$, and ϕrec $= (x, -x, y, -y, -x, x, -y, y)$. Quadrature in F_1 is achieved by States-TPPI[47] of ϕ2. For each value of t_2 a separate FID is recorded with the phase $\phi1 = (x, -x, -y, y)$, and the phases ϕ3 and ϕ4 are changed by 180°. For every successive t_2 increment ϕ1 and ϕrec are inverted.[48] Durations and strengths of the gradients (sine-bell) are g1 = (1.1 ms, 11 G/cm), g2 = (0.95 ms, 5 G/cm), g3 = (1.3 ms, 13 G/cm), g4 = (1.5 ms, −17 G/cm), g5 = (0.6 ms, −13 G/cm), g6 = (0.6 ms, 9 G/cm), and g7 = (0.6 ms, 15 G/cm).

while Figure 1b shows the DQ version of the HNCA experiment, which connects the ^1HN_i and $^{15}N_i$ nuclei to the sum of the chemical shifts of the $^{13}C^{\alpha}_i$ and $^{13}C^{\alpha}_{i-1}$ spins. The transfer steps for the intra- and DQ-HNCA experiments can be summarized as follows:

intra-HNCA

$$^1HN_i \xrightarrow{J_{HN}} {}^{15}N_i \xrightarrow[J_{NC'}]{J_{NC^a}} {}^{13}C^{\alpha}_i\,[t_1] \xrightarrow[J_{NC'}]{J_{NC^a}} {}^{15}N_i\,[t_2] \xrightarrow{J_{HN}} {}^1HN_i\,[t_3] \quad (1)$$

DQ-HNCA

$$^1HN_i \xrightarrow{J_{HN}} {}^{15}N_i \xrightarrow{J_{NC^a}} {}^{13}C^{\alpha}_i\,{}^{13}C^{\alpha}_{i-1}\,[t_1] \xrightarrow{J_{NC^a}} {}^{15}N_i\,[t_2] \xrightarrow{J_{HN}} {}^1HN_i\,[t_3] \quad (2)$$

In what follows, the relevant coherence transfer pathways in the two experiments are briefly described. Amide proton magnetization is transferred to the directly attached ^{15}N spin. During the following delay $2\tau_b$, evolution due to the one-bond and two-bond J_{NC^a} couplings occur. In addition the $^1J_{NC'}$ coupling is also active in the intra-HNCA experiment. A careful choice of $2\tau_b$ leads to the generation of the desired terms $4N_xC^{\alpha}(i)_zC^{\alpha}(i-1)_z$ in the DQ experiment and $8N_xC^{\alpha}(i)_zC^{\alpha}(i-1)_zC'_z$ in the intra-HNCA sequence (point a). The single-antiphase terms $2N_yC^{\alpha}(i)_z$ and $2N_yC^{\alpha}(i-1)_z$, used in the conventional HNCA experiment, are suppressed using the pulsed field gradient[34] applied after the ^{15}N 90° pulse at point a. In the DQ experiment (Figure 1b) a 90° pulse on $^{13}C^{\alpha}$ then creates multiple-quantum terms, the ^{13}C DQ coherence part of which is subsequently chemical shift labeled before it is transferred back to the ^{15}N spin. The ^{15}N frequency is then encoded during $2T_N$, and magnetization finally returned to the amide proton using a TROSY-type scheme, thus ensuring the most benefit from the slowly relaxing ^{15}N and ^1H components. On the other hand, in the case of the intra-HNCA experiment (Figure 1a), the coherence created at time point a is first converted via the carbonyl spin into $8N_zC^{\alpha}(i)_zC^{\alpha}(i-1)_zC'_x$. At this stage the dependence on the longitudinal operator $C^{\alpha}(i-1)_z$ is removed through refocusing via the one-bond $^1J_{C^aC'}$ coupling constant to create the term $4N_zC^{\alpha}(i)_zC'_y$ at point b. This step concludes the filter element which selects the intraresidue component, so that during t_1 only the chemical shift of the $^{13}C^{\alpha}_i$ is encoded. The final ^{15}N-CT[19,20] evolution period $2T_N$ involves simultaneous refocusing via the $^1J_{NC'}$ and $^1J_{NC^a}$ couplings and is followed by transfer back to the amide proton. In Figure 1 this is shown as a TROSY-type ST2-PT.[31] However, in principle other published TROSY schemes[16,17,35−37] can be implemented in the pulse sequences.

Several features in the new experiments require closer inspection. While in deuterated proteins the conventional 3D HNCA is among the most sensitive triple-resonance experiments available for the assignment of backbone resonances, one of its drawbacks is that it is often not possible to distinguish between the intra- and interresidue correlations as the one-bond and two-bond J_{NC^a} coupling constants can be of comparable magnitudes and therefore give similar signal intensities. Furthermore, the similarity in the magnitudes of the two $^{1,2}J_{NC^a}$ coupling constants also leads to a compromise in the achievable signal intensity of both cross-peaks because of attenuation by the passive coupling. Figure 2a depicts the amount of ^{15}N antiphase coherence which is generated in an HNCA experiment under the evolution of the active and the passive $^{1,2}J_{NC^a}$ couplings, taken as 11 and 7 Hz, respectively. Even in the absence of relaxation, attenuation resulting from the presence of the passive coupling keeps the transfer efficiency below 70% for the intraresidue pathway. In contrast to this, ^{15}N coherence

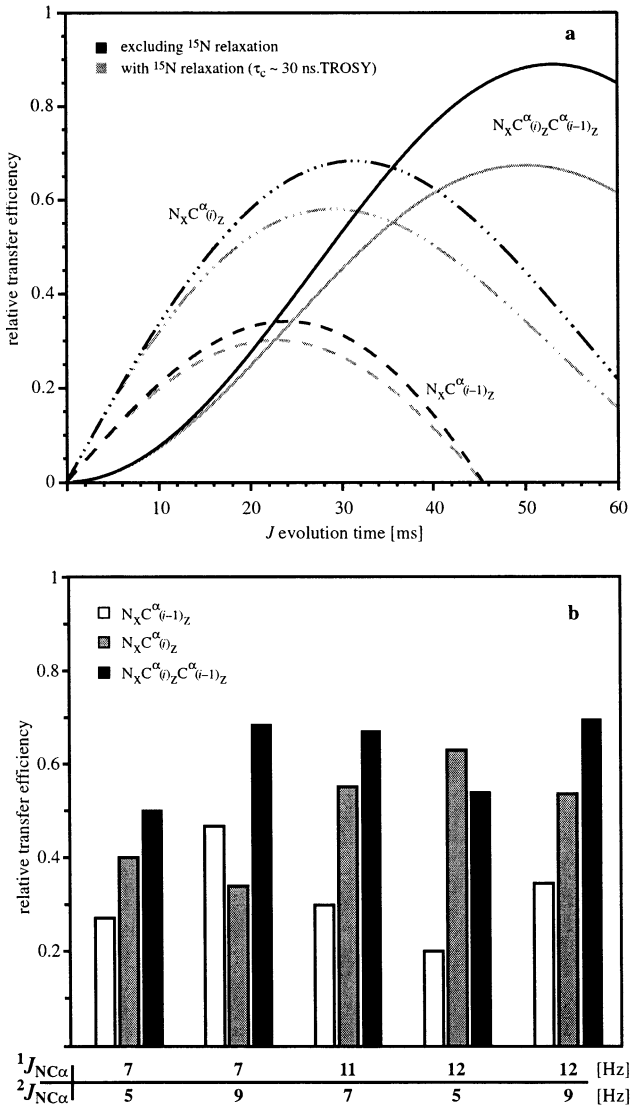

Figure 2. Generation of ^{15}N coherence antiphase to $^{13}C^{\alpha}_i$ and/or $^{13}C^{\alpha}_{i-1}$ through evolution of the $^1J_{NC^a}$ and $^2J_{NC^a}$ couplings. (a) Buildup as a function of the evolution time, using average values for the $^1J_{NC^a}$ (11 Hz) and $^2J_{NC^a}$ (7 Hz) couplings, both in the absence of relaxation (black lines) and including attentuation by relaxation (gray lines), assuming the ^{15}N TROSY transition of a 30 ns tumbling protein at 800 MHz ($R_2 = 8$ Hz). The double-antiphase term is used in the new intra-HNCA and DQ-HNCA (solid lines), while the single-antiphase terms lead to the intraresidue (dashed−dotted lines) connections in an HNCA spectrum, and the sequential connections (dashed lines) in the HN(CO)CA or the HNCA spectra. (b) Effect of variations in the size of $^{1,2}J_{NC^a}$ on the amount of antiphase coherence created with average evolution periods of 23 ms (single antiphase) and 52 ms (doubly antiphase). The interresidue (white columns), intraresidue (gray column), and double-antiphase (black columns) intensities are shown grouped by the various coupling constant size combinations considered.

(34) Bax, A.; Pochapsky, S. S. *J. Magn. Reson.* **1992**, *99*, 638−643.
(35) Czisch, M.; Boelens, R. *J. Magn. Reson.* **1998**, *134*, 158−160.
(36) Weigelt, J. *J. Am. Chem. Soc.* **1998**, *120*, 12706−12706.
(37) Rance, M.; Loria, J. P.; Palmer, A. G. *J. Magn. Reson.* **1999**, *136*, 92−101.

which is doubly antiphase to the two $^{13}C^{\alpha}$ spins, generated as the result of having both couplings active, is produced in higher quantity. Despite the fact that the transfer maximum is reached at a noticeably longer time point, calculations indicate that, even when considering relaxation in a ^{15}N TROSY experiment, for a large protein ($\tau_c \approx 30$ ns), the amount of the doubly antiphase term generated is still comparable to the situation in the conventional HNCA experiment (Figure 2a). Both ^{15}N transfer periods $2\tau_b$ and $2T_N$ in the DQ-HNCA are adjusted to benefit most from this advantageous in-phase/double-antiphase interconversion. Therefore, the DQ-HNCA experiment will still have reasonable sensitivity despite the 50% reduction of the signal intensity through selection of the DQ part of the multiple-quantum coherence generated at point a (Figure 1b). As a further advantage, due to the extended *J* transfer periods, this experiment can be recorded with significantly higher resolution in the ^{15}N dimension than is normally possible.

The optimized length of the *J* evolution period $2\tau_b$ shown in the pulse sequences of Figure 1 was set to 23 ms in the conventional experiments and to 52 ms in the two novel sequences. These values were determined from Figure 2a, in which we assume the average $^{1,2}J_{NC^a}$ coupling constants are 11 and 7 Hz, respectively. They also take into account ^{15}N TROSY relaxation for a deuterated macromolecule tumbling with a correlation time of 30 ns. In reality, the *J* couplings are more likely to vary between 5 and 9 Hz (^2J) and 7 and 12 Hz (^1J). These variations affect the transfer functions of Figure 2a and result in deviations from the average intensities shown. The impact of these *J* variations can be estimated from Figure 2b, where the relative transfer efficiencies of the single-interresidue, single-intraresidue, and doubly antiphase coherences are displayed for different combinations of ^1J and ^2J, assuming *average* evolution times of 23 ms (for singly antiphase) and 52 ms (for doubly antiphase), respectively. Clearly, the singly and doubly antiphase terms respond somewhat differently to variations in the size of the two coupling constants. However, the simulations also show that the range of intensity changes is similar for all three transfer pathways. For a given combination of coupling constants the transfer efficiency of the doubly antiphase coherence always remains higher than for the interresidue case. This favorable situation is also true for the intraresidue pathway, except for one case, where the active coupling is large (e.g., 12 Hz) and the passive coupling is small (e.g., 5 Hz) (Figure 2b). With increasingly fast relaxation of the ^{15}N nucleus all three transfer efficiencies are reduced, but their spread due to *J* variations decreases. A comparison between data simulated excluding relaxation and the set displayed in Figure 2b with $\tau_c \approx 30$ ns ($R_2 \approx 8$ Hz) indicates an approximate 10−20% reduction in the spread of transfer efficiencies due to *J* variations (data not shown).

The ambiguity in the HNCA spectrum is normally resolved by recording a complementary HN(CO)CA experiment from which the interresidue connections can be selectively determined. To achieve the necessary sensitivity, larger proteins typically require the implementation of TROSY-type transfer schemes for ^{15}N and ^1HN spins. These benefit most from the highest available magnetic fields, 800 or 900 MHz, where carbonyl transverse relaxation in large proteins starts to become prohibitively fast. Carbonyl transverse relaxation is dominated by the chemical shift anisotropy mechanism, which is approximately proportional to both the size of the protein and the square of the field strength employed. Its detrimental effect on the sensitivity of the HN(CO)CA experiment is particularly pronounced because it contains two periods during which carbonyl transverse relaxation is active. The intra-HNCA experiment is less sensitive than a conventional HNCA experiment, because it incorporates a single period ($2T_c$) where the carbonyl magnetization is transverse (see Figure 1a). But the loss sustained while the carbonyl magnetization is transverse is less pronounced than in the HN(CO)CA spectrum. In addition, the loss due to carbonyl relaxation is partly recovered through the higher efficiency of the ^{15}N coherence transfer where both J_{NC^a} couplings are active.

Results and Discussion

The transfer efficiencies of the two new intra-HNCA and DQ-HNCA experiments as well as the previously described TROSY versions of the HNCA,[14] HN(CO)CA,[15] and sequential-HNCA[24] experiments were simulated for a range of correlation times at static magnetic field strengths between 500 and 900 MHz (Figure 3b). Our aim was to provide a comparison of the performance of these experiments and to predict their behavior for proteins with correlation times longer than that of the experimental sample (see Figure 3). With increasing correlation times the sensitivity of the HN(CO)CA experiment drops away rapidly, particularly at higher magnetic field strengths (see Figure 3b). In addition, it is the only experiment which deteriorates with an increase in the magnetic field strength. Consequently, at a correlation time of >35 ns at 800 MHz, the $i - 1$ cross-peak in the HNCA experiment is detected with greater sensitivity as compared to the HN(CO)CA cross-peak. Nevertheless, in absolute terms the sequential connection is still weak, ~20% intensity of the intraresidue HNCA cross-peak. Because the intraresidue HNCA cross-peak remains intense, obtaining the interresidue connection for larger proteins clearly represents the limiting step in any assignment protocol. This problem can be overcome by utilizing the more sensitive DQ-HNCA experiment proposed here. Once the corresponding intraresidue connection has been determined through, for example, the intra-HNCA experiment, the correct $i - 1$ information can readily be obtained from the DQ experiment by subtraction of the two chemical shifts. Both the intra- and the DQ-HNCA experiments benefit from the highest magnetic field strength currently available, and simulations suggest that beyond 20 ns they should become more sensitive than the HN(CO)CA experiment, and thus provide a useful assignment strategy for larger proteins.

Due to the longer J_{NC^a} transfer periods, the new experiments are sensitive to faster ^{15}N relaxation and so do require high levels of deuteration. The relaxation rates of the slower relaxing TROSY coherence $N_{tr}H^{\beta}$ used in the simulations of Figures 2 and 3 were calculated by including dipole−dipole contributions from residual amide protons, as found in a typical α-helical environment. Due to the lower proton density, relaxation of the same coherence in a β-sheet environment should be slower, and would lead to slightly improved performance of all the experiments shown in Figure 3.

The two triple-resonance 3D experiments, intra- and DQ-HNCA, were tested at 800 MHz on a highly deuterated sample

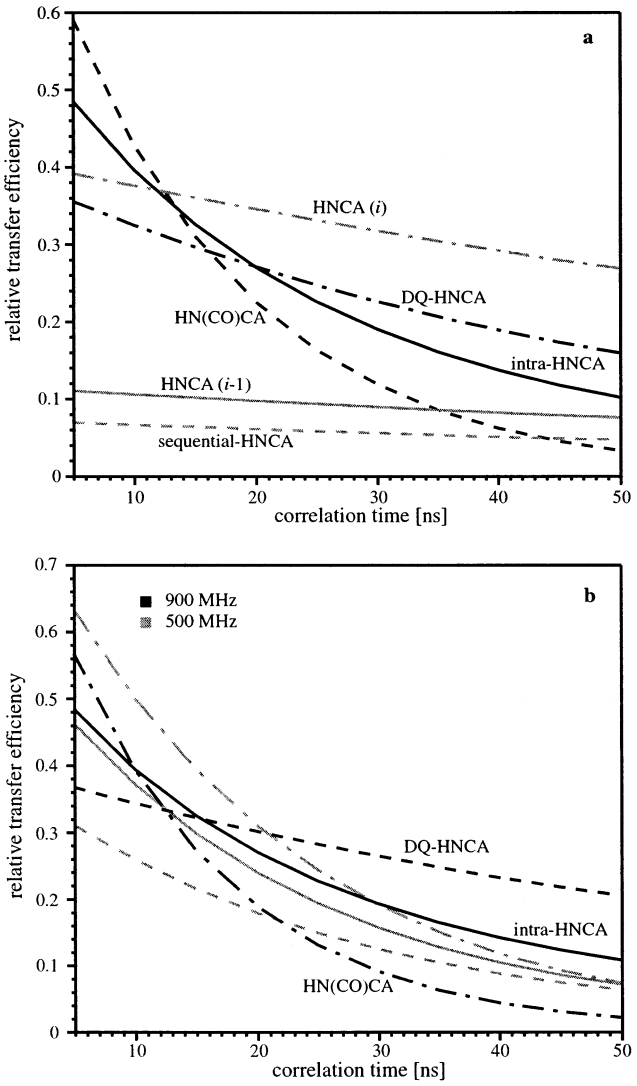

Figure 3. Calculated transfer efficiencies of triple-resonance TROSY NMR experiments as a function of the correlation time for a side-chain-deuterated protein. (a) Comparison at 800 MHz of the HNCA[14] (intraresidue *i* peak) (gray dashed−dotted line), DQ-HNCA (black dashed−dotted line), intra-HNCA (black solid line), HN(CO)CA[15] (black dashed line), HNCA (interresidue $i - 1$ cross-peak) (gray solid line), and sequential-HNCA[24] (gray dashed line) experiments. (b) Comparison of the effect of the magnetic field strength of 500 MHz (gray lines) versus 900 MHz (black lines). The intra-HNCA experiment is illustrated by solid lines, the DQ-HNCA by dashed lines, and the HN(CO)CA by dashed−dotted lines.

of H-Ras (1−171)-GDP at 4 °C. Under these conditions the correlation time of the protein was 28 ns as determined by the ^{15}N T_1/T_2 ratio,[38] i.e., approximately representative of a 60 kDa protein at room temperature. For comparative purposes 3D HNCA,[14] HN(CO)CA,[15] and sequential-HNCA[24] experiments were recorded under the same conditions. Using the intra- and DQ-HNCA spectra, 96% of the residues were successfully reassigned at 4 °C. With the new approach, four additional sequential connections could be made which were not possible using the HN(CO)CA experiment. In two cases the interresidue peak in the HN(CO)CA spectrum was missing, while in two further situations, overlap in the corresponding ^{1}HN/^{13}C$^{\alpha}$ plane of the HNCA spectrum, combined with missing HN(CO)CA assignments, led to ambiguity. For the remaining more problematic regions, where low sensitivity was an issue, the HNCA/HN(CO)CA method also failed to give a conclusive result.

The quality of data which could be obtained using the 1.0 mM sample of H-Ras is shown in Figure 4, where strip plots of the DQ-HNCA/intra-HNCA experiments are compared with those from the corresponding HNCA/HN(CO)CA spectra for residues Asp 154 to Tyr 157. Each of the experiments was run at 800 MHz for 29 h. In the displayed spectra the HN(CO)CA cross-peaks are clearly the least intense, ultimately limiting the efficiency with which the sequential assignment can be pursued. The superior sensitivity of the matching DQ-HNCA resonances over both the HN(CO)CA cross-peaks and $i - 1$ correlations in the HNCA spectrum is obvious. As expected, the correlations in the intra-HNCA spectra are slightly weaker than in the HNCA spectrum, but still good enough not to impede the assignment procedure. In return for this slightly lower sensitivity, the intra-HNCA experiment has the advantage of reduced spectral crowding in the ^{13}C dimension, because only one cross-peak per residue is observed. In Figure 4 the cross-peak connectivities are indicated by dashed lines, while two problem regions hindering the sequential assignment procedure using HNCA/HN(CO)CA spectra are highlighted by the dashed boxes. In one case the exact ^{1}HN shift of Lys 104 cannot be determined from the HNCA experiment because its *i* resonance overlaps closely with the $i - 1$ peak of Asp 154. In the other case the HNCA does not resolve the ^{13}C$^{\alpha}$ shift of Ala 155, as its *i* and $i - 1$ peak are almost degenerate. In neither of the two cases could the situation be resolved by improved data processing. However, neither ambiguity exists in the intra-HNCA experiment. These examples represent two general situations where the increased ^{13}C resolution of the intra-HNCA experiment can be very useful. This is particularly significant when using automatic assignment procedures, where the accurate determination of peak shift positions is a stringent requirement.

As the resonances in the DQ experiment appear at the sum of the ^{13}C$^{\alpha}_{i}$ and ^{13}C$^{\alpha}_{i-1}$ shifts, at first sight this information may seem inconvenient to use. Nevertheless, the sequential ^{13}C$^{\alpha}_{i-1}$ single-quantum shift can easily be obtained by subtraction of the corresponding ^{13}C$^{\alpha}_{i}$ shift via re-referencing of the spectrum. While the assignment is in progress, this procedure needs to be repeated for every residue and is therefore best automated in the assignment software. In ANSIG[29] this has been implemented, such that any selected cross-peak is shifted "on-the-fly" to its correct position. In Figure 4, the displayed ^{13}C$^{\alpha}_{i-1}$ resonances have already been moved to their correct single-quantum positions. Once this correction has been made, the assignment of the two 3D spectra is straightforward and can proceed in the usual manner by matching the ^{13}C$^{\alpha}$ shifts for the ^{1}HN spins from the *i* and $i + 1$ residues (Figure 4).

By comparison with the conventional HNCA spectrum, the intra version of the experiment results in a reduction of spectral crowding because only half the number of peaks are present. If required, the spectral dispersion in the intra-HNCA experiment can be increased further by the introduction of a carbonyl evolution period in a fourth dimension. This does not affect the length of the pulse sequence as the carbonyl shift labeling is implemented in a constant time period. The resulting 4D spectrum can then be used in conjunction with either the HNCO$_{i-1}$CA$_i$ experiment suggested by Konrat et al.[39] or an

(38) Kay, L. E.; Torchia, D. A.; Bax, A. *Biochemistry* **1989**, *28*, 8972−8979.

(39) Konrat, R.; Yang, D. W.; Kay, L. E. *J. Biomol. NMR* **1999**, *15*, 309−313.

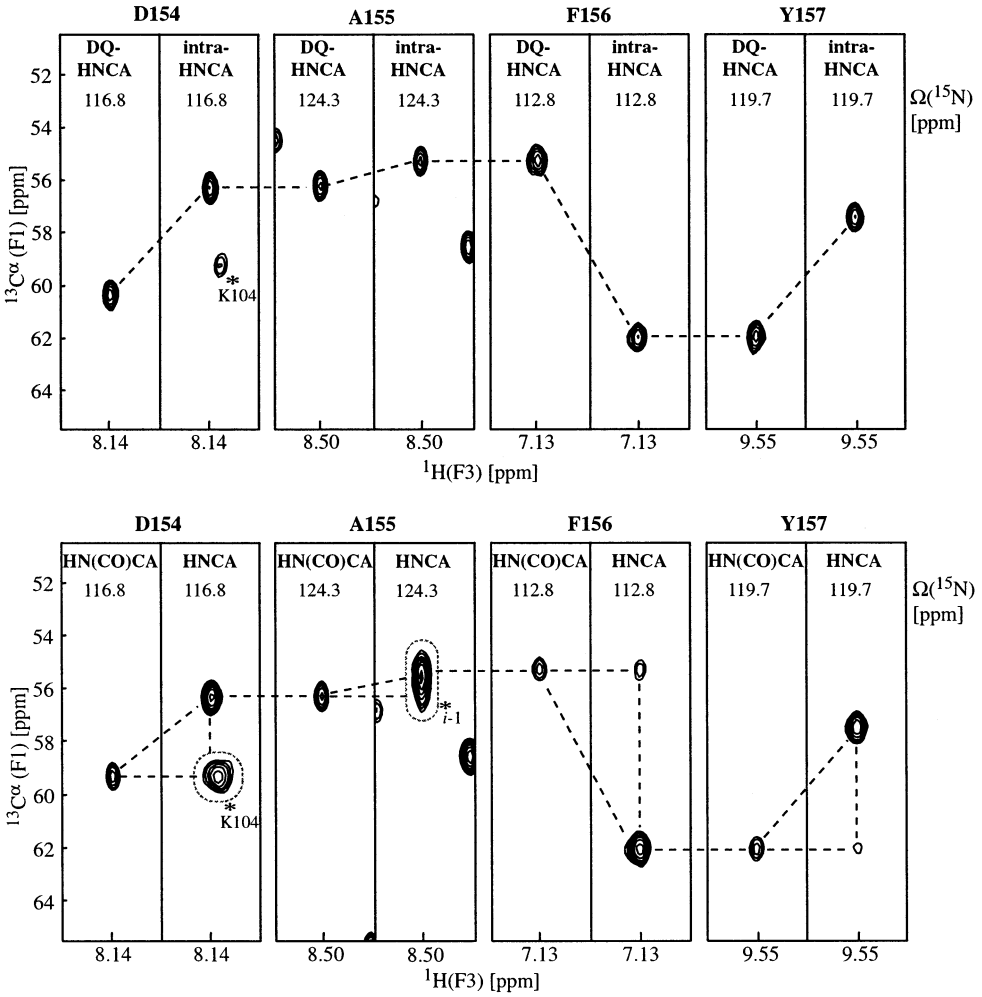

Figure 4. Contour strip plots of the $^{1}HN/^{13}C^{\alpha}$ planes of residues Asp 154 to Tyr 157 in H-Ras (1−171)-GDP. Comparison of the 3D intra-HNCA and 3D DQ-HNCA spectra with the corresponding HNCA/HN(CO)CA planes recorded on a 1.0 mM sample of ^{15}N, ^{13}C, ^{2}H [Ile(δ_1 only), Leu, Val]-methyl-protonated H-Ras (1−171) at 4 °C (τ_c = 28 ns). The ^{13}C chemical shifts in the DQ experiment have already been corrected to the single-quantum $i - 1$ shifts, so that the sequential backbone assignment can proceed in the usual way, indicated by dashed lines. Two problematic regions which result in ambiguity in the HNCA/HN(CO)CA-based assignment are highlighted by gray dashed outlines, with the interfering cross-peaks marked by an asterisk (K 104 and $i -$ 1 of A 155). The ambiguity is removed in the intra-HNCA/DQ-HNCA approach.

HNCACO[22] spectrum, with the additional advantage of uniquely observing the intra-connections. Despite the larger ^{13}C chemical shift range in the DQ-HNCA spectrum, the same spectral widths were used in all experiments, leading to identical spectral resolution for the same total experiment time. Hence, it is necessary to adjust the initial delay of the $^{13}C^{\alpha}$ evolution period to obtain a 90°, −180° phase correction so that folded resonances can be recognized by their opposite signs.

Both new experiments give very clean spectra, and despite the expected small variations in the magnitude of the $^{1,2}J_{NC^a}$ coupling constants, the suppression of the interresidue component in the intra-HNCA is highly efficient. This is mostly attributable to the fact that the $^{2}J_{C^aC'}$ coupling constant is at least 20 times smaller than $^{1}J_{C^aC'}$, thus providing efficient suppression of the unwanted coherences in the step where the carbonyl spin is transverse (Figure 1a).

To evaluate the sensitivity of the two new experiments, the signal-to-noise (S/N) distribution of 140 cross-peaks was compared with the results of a HN(CO)CA[15] spectrum and of a sequential-HNCA spectrum, similar to the previously published experiment.[24] The average S/N ratios were calculated for each of the different experiments. At 800 MHz the average S/N ratios for both the DQ-HNCA and the intra-HNCA experiments were 41, while for the HN(CO)CA and sequential-HNCA spectra they were 28 and 15, respectively. To prevent bias by the few very intense peaks, those with S/N > 110 were excluded from this average calculation. Clearly, the new experiments compare favorably, with their peak distribution shifted toward higher signal-to-noise values. This is in agreement with the higher overall sensitivity predicted by the simulations. To investigate the impact of the static magnetic field strength, each experiment was repeated at 600 MHz. All experiments except the HN(CO)CA benefit from the higher sensitivity at 800 MHz. At 600 MHz the sensitivities of the DQ-HNCA, intra-HNCA, and HN(CO)CA experiments were comparable, with an average S/N value of approximately 33, while the S/N of the sequential-HNCA experiment is still only 13.

The high sensitivity of the intra-HNCA experiment shows that the loss sustained through carbonyl relaxation can be compensated through the higher efficiency of the modified out-and-back ^{15}N coherence transfer scheme. As the intra-HNCA has only one carbonyl transverse period, it benefits from higher magnetic fields. Equally, the more efficient buildup of doubly antiphase coherence during the ^{15}N periods of the DQ-HNCA

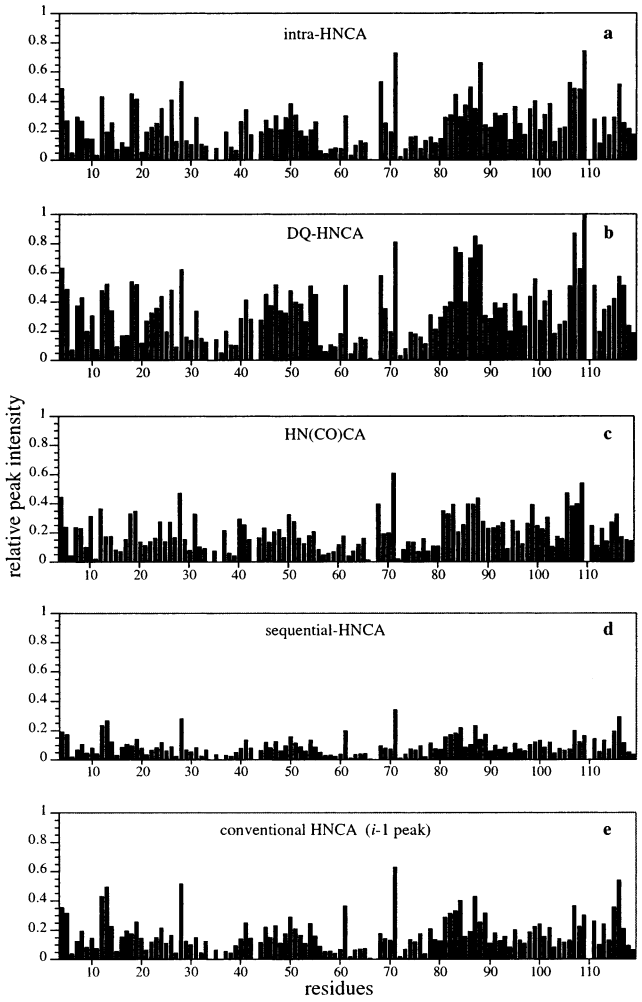

Figure 5. Comparison of peak intensities for residues 4−120 of H-Ras (1−171) in the intra-HNCA, DQ-HNCA, HN(CO)CA, sequential-HNCA, and conventional HNCA ($i - 1$ resonance) experiments. All the peak intensities are displayed relative to that of Val 109 in the DQ-HNCA to allow a direct comparison between the different experiments.

experiment compensates for the 50% signal loss inflicted by the double-quantum coherence selection mechanism. The HN(CO)CA experiment, however, is attenuated in two periods of increasingly fast carbonyl relaxation so that the overall sensitivity deteriorates at field strengths beyond 500 MHz. It is important to note that the elongated ^{15}N coherence transfer periods require slow ^{15}N transverse relaxation and therefore work best under TROSY conditions at the highest magnetic field available and in combination with high levels of side chain deuteration.

To allow a direct sensitivity comparison and to obtain a better estimate of how changes in ^{15}N relaxation rates and J_{NC^a} coupling constants alter the performance of the new experiments, the relative peak intensities for residues 4−120 of ras p21 from the intra-HNCA, DQ-HNCA, HN(CO)CA, sequential-HNCA, and conventional HNCA ($i - 1$ resonance) experiments were compared (Figure 5). This residue-by-residue comparison illustrates the superior sensitivity of the new experiments. While the relative signal intensities in the DQ-HNCA, intra-HNCA, and HN(CO)CA experiments are similar, the signals are dispersed over a wider range of S/N in the two new experiments. In part, this may result from the use of longer evolution periods, which have higher sensitivity to a nonuniform distribution of ^{15}N relaxation rates. For example, the DQ-HNCA contains two elongated transfer periods, which might explain why the performance of this experiment is slightly reduced in comparison to the theoretical predictions in Figure 3. In general, performance variations do not seem to have an obvious correlation to changes in secondary structure or to the residual proton density resulting from incomplete deuteration. More importantly, however, residues that show strongly reduced intensities in the HN(CO)CA spectrum benefit from the improved sensitivity of the new experiments. While an improved overall experiment performance is very desirable, an assignment procedure is typically limited by those residues with low experimental sensitivity. A direct comparison in Figure 5 shows that out of 21 residues with a S/N below 15 in the HN(CO)CA, 20 have improved sensitivity in the new experiments. The improvements are generally larger than 20% and are obtained over the entire achievable sensitivity range. A similar trend is observed for residues 141−171 of the protein (data not shown).

The sensitivity trends predicted by the theoretical transfer functions depicted in Figure 3 are confirmed by the analysis of the experimental data recorded at 800 and 600 MHz, indicating that the calculations offer an adequate representation of the various experiments. The calculations suggest that the intra-HNCA and DQ-HNCA experiments should enable assignment of proteins with correlation times well beyond 50 ns and should give data with increased sensitivity. For the backbone assignment of large proteins with several hundred residues one will always have to record several complementary experiments. Modifications can be made to the HNCACB[9,40] pulse sequence, in a manner similar to that of the intra-HNCA, to result in an experiment which allows the selective observation of intraresidue $^{13}C^{\alpha}_i$ and $^{13}C^{\beta}_i$ shifts. The newly introduced scheme, which makes use of doubly antiphase coherence, is thus general and can be incorporated into a wide range of pulse sequences.

While larger deuterated proteins benefit from TROSY-type pulse sequences, conventional INEPT implementations of the same experiments are preferably used with faster tumbling proteins. An INEPT-style implementation of the intra-HNCA which uses ^{1}H decoupling during the ^{15}N and ^{13}C transfer periods, was tested at 25 °C on a protonated sample of human ubiquitin. At 600 MHz the peak intensities are on average only approximately 15−20% weaker than those of the HNCA *i* peak (data not shown). In such cases the intra-HNCA can be used as a complementary experiment to the HNCA experiment. In addition the intra-HNCA experiment can be recorded with a higher resolution in the ^{15}N dimension, if the ^{15}N chemical shift labeling period is moved to the longer first J_{NC^a} evolution delay ($2\tau_b$ in Figure 1a), providing a further benefit. This modified chemical shift labeling scheme can easily be implemented by concerted simultaneous incrementation of the three 180° pulses

(40) Wittekind, M.; Mueller, L. *J. Magn. Reson., Ser. B* **1993**, *101*, 201−205.
(41) Kupce, E.; Boyd, J.; Campbell, I. D. *J. Magn. Reson., Ser. B* **1995**, *106*, 300−303.
(42) Piotto, M.; Saudek, V.; Sklenar, V. *J. Biomol. NMR* **1992**, *2*, 661−665.
(43) Shaka, A. J.; Keeler, J.; Freeman, R. *J. Magn. Reson.* **1983**, *53*, 313−340.
(44) McCoy, M. A.; Mueller, L. *J. Am. Chem. Soc.* **1992**, *114*, 2108−2112.
(45) Emsley, L.; Bodenhausen, G. *Chem. Phys. Lett.* **1990**, *165*, 469−476.
(46) Bohlen, J. M.; Bodenhausen, G. *J. Magn. Reson., Ser. A* **1993**, *102*, 293−301.
(47) Marion, D.; Ikura, M.; Tschudin, R.; Bax, A. *J. Magn. Reson.* **1989**, *85*, 393−399.
(48) Kay, L. E.; Keifer, P.; Saarinen, T. *J. Am. Chem. Soc.* **1992**, *114*, 10663−10665.

in the $2\tau_b$ period of Figure 1a, while at the same time keeping the pulses in the $2T_N$ period constant. It should be noted, however, that this is not applicable to the TROSY implementations, where chemical shift labeling must occur before the back-transfer of the orthogonal coherence components prior to acquisition.

In contrast to this, however, the DQ-HNCA experiment when recorded on protonated samples suffers from the faster dipolar relaxation of the double-quantum coherence in the ^{13}C evolution period, making this experiment predominantly useful for deuterated proteins. In the case of ubiquitin the sensitivity of the DQ-HNCA is between 20% and 30% lower than for the corresponding $i - 1$ cross-peaks in the conventional HNCA. For large deuterated proteins only molecular fragments where both $^{13}C^{\alpha}$ positions are deuterated contribute to the detected signal. The sensitivity of this experiment is therefore attenuated by the square of the level of deuteration, while for all the other experiments this dependence remains linear. Levels of deuteration of the $^{13}C^{\alpha}$ position higher than 90% are therefore generally needed to prevent excessive loss of signal. Here spectra with a higher resolution in the ^{15}N dimension can be recorded with both the INEPT and TROSY versions of the experiment.

Conclusions

The backbone assignment process of very large proteins can be severely hindered by the low sensitivity with which the sequential $i - 1$ correlation is detected at high magnetic field strengths. We present two new sensitive TROSY-based experiments that when used together alleviate this problem, allowing sequential assignment of deuterated proteins with better sensitivity and higher resolution. An intra-HNCA experiment where the intraresidue $^{13}C^{\alpha}_i$ connection is selectively observed, in combination with a DQ-HNCA experiment, allows the sequential assignment. Experimental data for a deuterated protein tumbling with the correlation time expected of a ~60 kDa protein are presented, and show that the new approach is superior to traditional methods which involve use of the HN(CO)CA- or sequential-HNCA-type experiments to obtain the desired interresidue information. Theoretical predictions are made for larger slower tumbling proteins, and these suggest that the new approach should be applicable for proteins with correlation times >50 ns.

Acknowledgment. We thank Dr. Minoru Hatanaka and Prof. Shigeyuki Yokoyama (Protein Research Genomic Sciences Centre, RIKEN, Yokohama, Japan) for preparing the H-Ras sample. We are grateful to Dr. Helen Mott, Dr. Katherine Stott, Dr. Peter Nielsen, and Abarna Thiru for stimulating discussions. The Cambridge Centre for Molecular Recognition is supported by the BBSRC and the Wellcome Trust.

JA025865M